Progress In Electromagnetics Research, Vol. 136, 157–173, 2013

DESIGN OF A COMPACT ULTRAWIDEBAND METAMATERIAL ANTENNA BASED ON THE MODIFIED SPLIT-RING RESONATOR AND CAPACITIVELY LOADED STRIPS UNIT CELL

Mimi A. W. Nordin[1, 2], Mohammad T. Islam[1, 2, *], and Norbahiah Misran[1, 2]

[1]Institute of Space Science (ANGKASA), Universiti Kebangsaan Malaysia, UKM Bangi 43600, Malaysia

[2]Department of Electrical, Electronic & Systems Engineering, Universiti Kebangsaan Malaysia, UKM Bangi 43600, Malaysia

Abstract—A new compact ultrawideband (UWB) patch antenna based on the resonance mechanism of a composite right/left-handed (CRLH) transmission line (TL) is proposed. The radiating element of the antenna is made from three left-handed (LH) metamaterial (MTM) unit cells placed along one axis, where each unit cell combines a modified split-ring resonator (SRR) structure with capacitively loaded strips (CLS). An analysis of the eigenfrequencies of these unit cells yields one- and two-dimensional dispersion diagrams, which correspond to a one-unit cell antenna and the three unit cell antenna, respectively. A trident feed and a slotted-partial ground plane are used to match the right- and left-handed (RH and LH) modes of the antenna, respectively. In addition, an analysis of the surface current distribution of the antenna shows that slots on the metallic area reduce the Q-factor. This reduction in the Q-factor results in a wide bandwidth of 189% at 3.7 GHz, which spans the UWB frequency range between 2.9–9.9 GHz. The total footprint of the antenna at the lowest frequency is $0.2\lambda_0 \times 0.2\lambda_0 \times 0.015\lambda_0$, where λ_0 is the free space wavelength. The gain of the antenna ranges between -1 to 5 dB throughout the frequency band.

1. INTRODUCTION

The Ultrawideband (UWB) communication technology poses a new challenge in antenna design due to the many design constraints

Received 7 October 2012, Accepted 5 January 2013, Scheduled 17 January 2013

* Corresponding author: Mohammad T. Islam (titareq@yahoo.com).

imposed by the technology. Furthermore, with UWB terminals becoming more prominent in consumer electronics, which require short-range and high data-rate connections, additional requirements must be considered. Key requirements of a UWB antenna include impedance matching for the frequency range between 3.1–10.6 GHz, a consistent gain over the matched frequency range, and a compact and inexpensive overall structure [1–4]. Although many frequency-independent antenna designs meet these requirements, the current literature suggests that a printed, low profile antenna design may be best, due to its ease of fabrication and its robust overall structure [5–9].

The recent discovery of left-handed metamaterials (LHMs) allows antennas to be designed with novel electromagnetic properties such as negative permittivity and permeability. When both permittivity and permeability are negative, backward wave propagation, where group velocity opposes phase velocity is possible. Many microwave devices such as broadband couplers, phase shifters and filters have been designed using LHMs to exploit their unique characteristics [10–16]. LHMs have also contributed to reductions in antenna size, as they display mode-dependent rather than size dependent resonance [17, 18]. Because LHMs do not exist in nature, they must be engineered to have these novel properties. Approaches for the creation of an LHM fall into two main categories: resonant and non-resonant [19]. Resonant approaches create an LHM by inducing the electric and magnetic dipole moments to achieve negative permittivity and permeability, respectively. However, structures designed using this approach suffer from narrow operating bandwidths due to the inherently high Q-factor of resonant structures [20]. An alternative approach creates an LHM by reactively loading a conventional transmission line (TL). An LHM TL can form a non-resonant structure that is generally described by the composite right/left-handed (CRLH) TL model, which takes into account the parasitic elements that arises from wave propagation in a conventional TL [21].

This paper presents a UWB metamaterial antenna. The antenna consists of three unit cells printed in a planar configuration. The behavior of the unit cells is analyzed using a resonant approach, while the behavior of the entire antenna structure is analyzed using a non-resonant TL approach. The antenna is then matched to a trident feed and a slotted partial ground plane. Finally, by analyzing the surface current distribution of the antenna, slots are introduced on the top layer to reduce the Q-factor and increase the bandwidth of the antenna. Section 2 presents the dispersion and resonance condition analyses of the unit cell. Section 3 presents one- and three-element antennas that meet the analytical characterization of the unit cells.

The advantage of a trident feed is also discussed. Section 4 presents the broadbanding method is used in the three-element trident-feed antenna. This section also presents the return loss and radiation profile of a fabricated prototype of the final antenna structure.

2. THE LHM UNIT CELL

The design of the UWB antenna begins with a study of the LHM unit cell. The objective is to obtain a unit cell design with resonance characteristics within the UWB frequency range of 3.1–10.6 GHz. The dispersion diagram, which is a plot of the phase velocity, β, versus the eigenfrequency of the structure, f, is used to determine whether this objective is satisfied. The dispersion diagram also indicates whethere the structure displays left-handed (LH) or right-handed (RH) characteristics by a negative or positive slope, respectively [21]. To meet the design objective, the frequencies in the dispersion relation that correspond to the resonance indices, m, should occur within the UWB frequency range. The resonance profile can then be obtained by sampling the dispersion diagram, as follows [21]:

$$\beta_m p = m\pi/2 \tag{1}$$

where

m = resonance index, 0, ± 1, ± 2, ... $\pm \propto$ and

p = physical length of the unit cell.

A full-wave analysis of the unit cell, using appropriate boundary conditions can be used to obtain the dispersion diagram. The simulation-based analysis treats the unit cells as individual resonators, which can be extended into an infinite structure or medium using the periodic boundary conditions. By parametrically changing the phase shifts between the periodic boundary (placed on the periphery of the unit cells and in the direction of wave propagation), a plot of eigenfrequencies versus phase shifts (which is phase velocity, β multiplied by p) can be obtained. This plot represents the dispersion diagram. In general, 1D and 2D dispersion diagrams are plotted for unit cells that are replicated in one and two directions, respectively [17]. In this paper, the initial unit cell is based on a split-ring resonator (SRR) structure. The SRR consists of two loops: a smaller loop within a bigger one, with slots incorporated onto each loop at opposite ends [22]. The SRR is a magnetically resonant structure that responds to a perpendicular magnetic field which can be used to create negative permeability. Gaps (or splits) added to the ring, introduce capacitance, which allows for the control of the resonant characteristic of the structure. The first unit cell is actually the modified rectangular

SRR shown in Figure 1. The modification is the closing of the loop on the outer ring, which reduces the series capacitance of the SRR. Furthermore, closing the outer ring enhances the coupling between the outer and inner ring, which enables a wide backward-wave passband [23]. The unit cell is built on top of an FR4 substrate with a dielectric constant, ε_r, of 4.6 and height, h, of 1.6 mm. The dimensions of the unit cell shown in Figure 1 are as follows: $L = 3.2$ mm, WSRR $= 4$ mm, $W_1 = 0.4$ mm, $W_2 = 1.6$ mm and $W_3 = 0.8$ mm. The dispersion diagram of the structure is plotted in red in Figure 2. The first resonant mode, shown in Figure 2(a), has a negative slope, is therefore an LH mode, and ranges 15.24 GHz to 11.91 GHz. The second resonant mode, shown in Figure 2(b), has a positive slope and is therefore RH and ranges from 15.24 GHz to 15.55 GHz. Both the LH and RH modes are operating above the UWB frequency range. Therefore, further modifications are required to lower the resonance profile of the proposed unit cell design.

Capacitance-loaded strips (CLS) were added to the modified SRR unit cell to bring the resonance profile within the UWB frequency range. CLS which act as electric dipoles are I-shaped striplines that mimic long metallic wires [24]. The combined structure (modified SRR and CLS) allows for simultaneous electric and magnetic resonance because the SRR resonates through a perpendicular magnetic field and the CLS (which is in essence an electric dipole) resonates through a parallel electric field [25]. The two resonance mechanism enables a lower resonance for the entire structure through the combined induced current [26]. The unit cell of the modified SRR with the additional

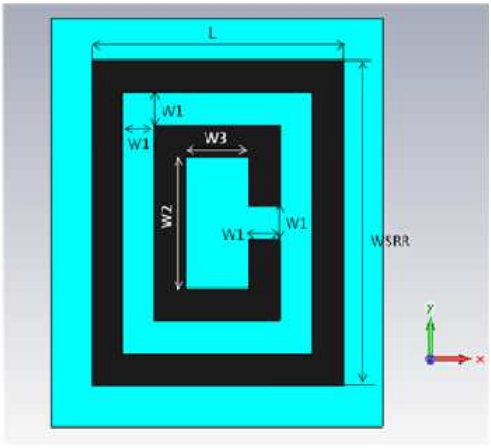

Figure 1. The modified SRR unit cell.

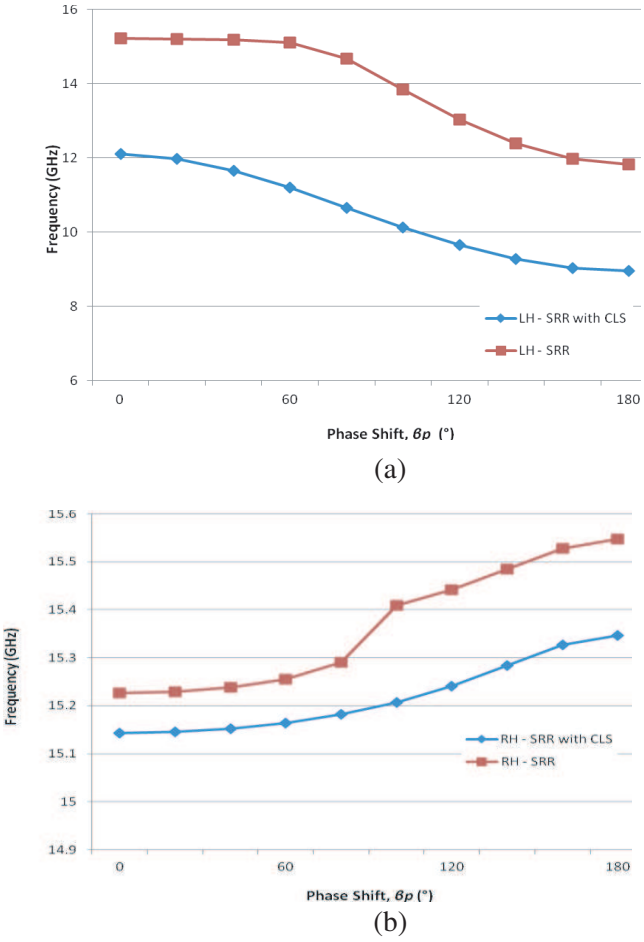

Figure 2. Comparison between the 2D dispersion diagrams of modified SRR unit cells (plotted in red) and modified SRR unit cells with CLS (plotted in blue), for the (a) left-handed (LH) and (b) right-handed (RH) modes.

CLS structure is shown in Figure 3. The SRR/CLS unit cell retains the dimensions of the SRR only structure described in Figure 1, except for the dimensions due to the addition of the CLS: WCLS = 5 mm, $W_4 = 0.5$ m and $W_5 = 3$ mm.

The dispersion diagrams of the modified SRR/CLS structure are plotted in blue in Figure 2. The resonance profile of the unit cell is lower for both the LH and RH modes. The first resonant mode is an

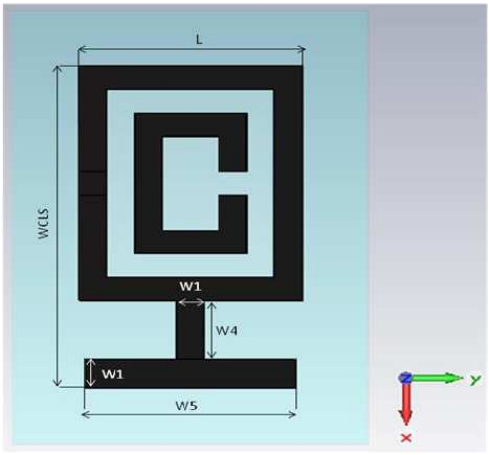

Figure 3. Front view of the modified SRR/CLS unit cell.

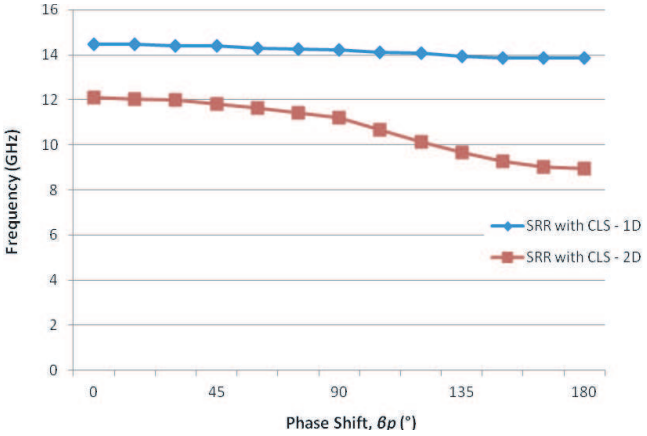

Figure 4. 1D dispersion diagram of the SRR/CLS unit cell.

LH mode, and ranges from 12.01 GHz to 9.01 GHz while the second resonant mode, is an RH and ranges from 15.14 GHz to 15.35 GHz. The resonance profile of the LH mode of the SRR/CLS structure is now within the UWB frequency range. The addition of the CLS to the modified SRR unit cell also decreases the amount of dispersion in the LH mode. This result can be seen in Figure 2(a), in which the gradient of the modified SRR/CLS curve is less than the gradient of the modified SRR curve.

A 1D dispersion diagram analysis was performed to determine

the effect of mode coupling in the SRR/ CLS unit cell structure. Figure 4 shows the comparison between the LH mode of this structure 1) without coupling (plotted in blue) and 2) with coupling (plotted in red). The coupling of the modes clearly lowers the resonance profile of the unit cell. Although because the 2D curve has a higher gradient than the 1D curve, the dispersion also increases.

3. THE MTM ANTENNA

The unit cells are themselves radiation sources due to the surface current that forms on them. The surface current is related to the magnetic and electric dipole moments of the SRR and CLS, respectively, by the following relationships [27]:

$$\overrightarrow{p_m} = \frac{\mu_0}{2} \int_s \overrightarrow{r} \times \overrightarrow{J_e}\left(r'\right) ds' \tag{2}$$

$$\overrightarrow{p_e} = \frac{j}{\omega} \int_s \overrightarrow{\nabla} \cdot \overrightarrow{J_e}\left(r'\right) ds' \tag{3}$$

where r is the displacement vector directed from the surface current element to the p_m/p_e calculation points, r' the current element position, and ds' the differential current carrying surface element.

The unit cell can be an efficient source of radiation when excited by its eigencurrents [27]. Therefore, the ability to excite the eigenfrequencies of a unit cell will enable its use as an effective radiating source. The design of the MTM antenna thus begins with the use of one unit cell as the radiating element, as shown in Figure 5(a). The footprint of the antenna is 11.5×13 mm. A quarter wave transformer was used to match the $120\,\Omega$ line that directly feeds the unit cell (width $= 0.4$ mm), with a $50\,\Omega$ line (width $= 3$ mm) that interfaces with the port. The dimensions of the feedline are as follows: $L_1 = 2.5$ mm, $L_2 = 2$ mm and $L_3 = 3$ mm. The number of expected resonance points is one, which corresponds to the resonance index $m = 0$. This number is obtained from the following equation, where N is the number of unit cells [21]:

$$\text{Number of resonance points} = 2N - 1 \tag{4}$$

The resonance frequency of the antenna can be obtained by sampling the 1D dispersion diagram in Figure 4 at $\beta_0 p = 0°$, as determined by Equation (1). The use of the 1D dispersion diagram is appropriate because the antenna is excited in only one direction from the feedline and does not experience any other excitation. The return loss, S_{11}, of the one-element antenna is shown in Figure 6. Although the loss is high, the antenna shows a resonance profile that is in good agreement

with the resonance predicted by the 1D dispersion diagram. The resonance of the antenna is at 13.71 GHz (−7.8 dB), while the 1D dispersion diagram (blue line in Figure 4) predicted a resonance at 14.48 GHz for $m = 0$.

Next, the same unit cell is used to construct a three element antenna, shown in Figure 5(b), where the three unit cells in the y-direction. Increasing the number of unit cells in the antenna results in more resonant points that can be sampled from the dispersion diagram and matched to form a wideband From Equation (5), the number of expected resonance points when using three unit cells is five, which corresponds to the resonance indices $m = 0, \pm 1$ and ± 2. By using Equation (1), the 2D dispersion diagram will be sampled as follows: 1) $m = 0$ at $\beta_0 p = 0°$, 2) the two first-order modes ($m = -1$ and $m = +1$) at $\beta_{-1} p = -90°$ and $\beta_{+1} p = +90°$ respectively and 3) the two second-order modes, ($m = -2$ and $m = +2$) at $\beta_{-2} p = -180°$ and $\beta_{+2} p = +180°$ respectively. The antenna structure directly interfaces the three unit cells to a trident-shaped feed, which effectively promotes an even field distribution [28] and the excitation of the unit cells. The space between the unit cells, d, and the trident feed width, W_6, was optimized to match the resonance frequencies predicted by the dispersion diagram. The total footprint of the antenna is 22 mm × 21 mm, and other dimensions of the antenna structure labeled in Figure 5(b) are as follows: $d = 1.9$ mm, $W_6 = 1$ mm, $W_7 = 2$ mm, $W_8 = 3.5$ mm, $W_9 = 11$ mm, $W_{10} = 10.5$ mm and $W_{11} = 3$ mm.

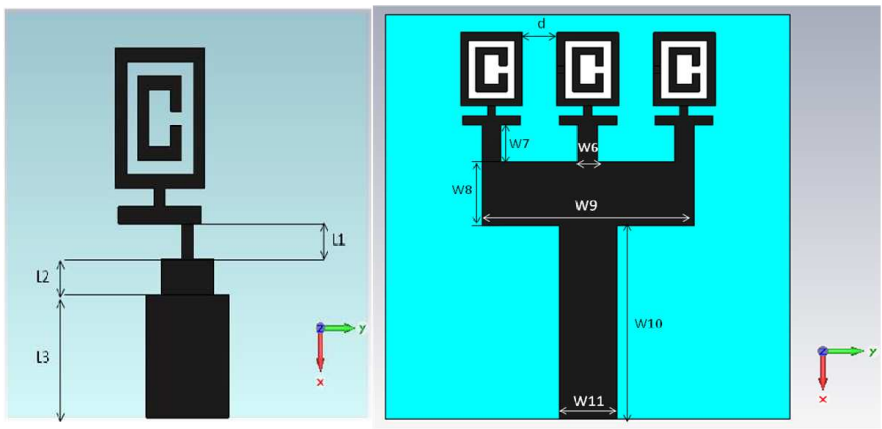

(a) (b)

Figure 5. (a) One element MTM antenna and (b) three-element MTM antenna.

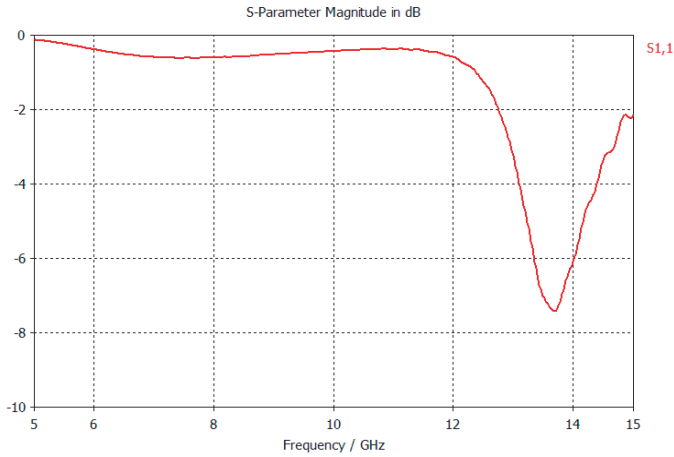

Figure 6. The return loss, S_{11}, of the one element MTM antenna.

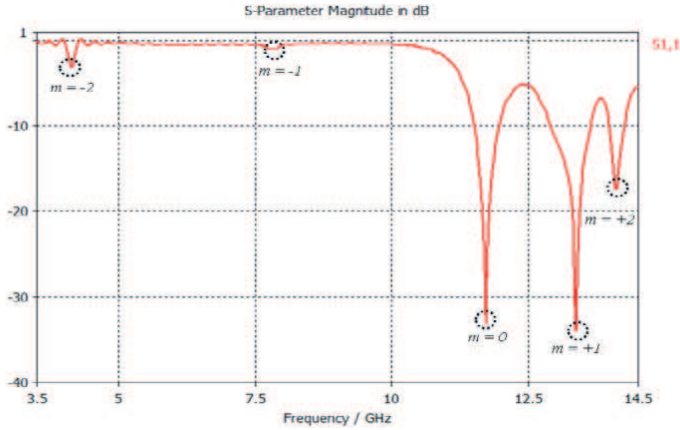

Figure 7. The return loss, S_{11}, of the three element MTM antenna.

The antenna structure was analyzed using the commercial EM solver Computer Simulation Technology (CST) and the return loss of the antenna and the pertinent resonance indices are shown in Figure 7. Table 1 lists and summarizes the resonance frequencies obtained from sampling the 2D dispersion diagrams in Figure 2, and from the full-wave simulation of the three-element antenna structure. The return loss analysis shows that the antenna is better matched at the higher resonance frequencies, which correspond to the zeroth order mode

Table 1. Resonance frequencies obtained from sampling the 2D dispersion diagram and from the full-wave simulation of the antenna structure.

	$m = 0$	$m = \pm 1$		$m = \pm 2$	
		m	f, GHz/dB	m	f, GHz/dB
2D Dispersion Diagra	12	+1	15.18	+2	15.36
		−1	10.8	−2	9.02
Full Wave Simulation of Antenn	11.76 (−33)	+1	13.47 (−34)	+2	14.09 (−17)
		−1	7.82 (−1)	−2	4.12 (−3)

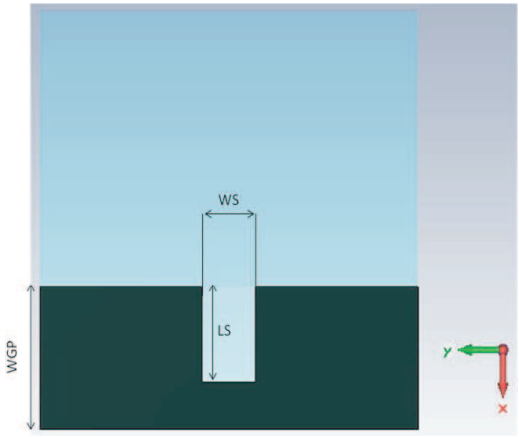

Figure 8. The bottom layer of the antenna structure.

$m = 0$ and the RH (positive) modes $m = +1$ and $+2$, with return losses below -10 dB. These resonance frequencies are also in good agreement with the eigenmode analysis of the unit cells at the corresponding modes indicating that the trident feed is effective in exciting the RH modes of the unit cells.

4. THE ULTRAWIDEBAND MTM ANTENNA

The bandwidth of an antenna is inversely related to the quality factor, Q [29, 30], which is a factor that characterizes the ratio between stored energy and radiated energy. Structures with a higher stored energy

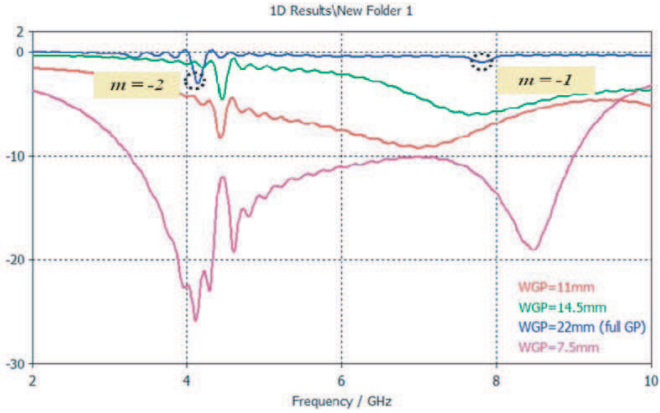

Figure 9. The effect of the size of the ground plane, WGP, on the return loss of the antenna.

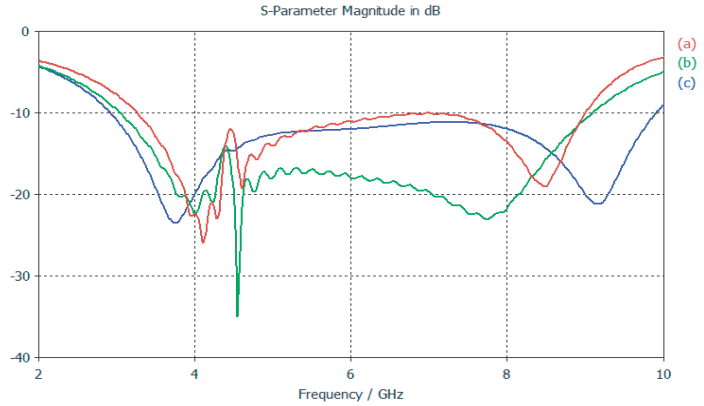

Figure 10. Comparisons between the return losses of (a) partial ground plane, $W_{GP} = 7.5\,\text{mm}$, (b) slotted partial ground plane, and (c) etched-out antenna on top of the slotted partial ground plane.

have a higher Q factor and therefore a narrower bandwidth. In an effort to improve the matching of the LH modes and increase the bandwidth of the antenna, a ground plane was used as an additional degree of freedom. A smaller ground plane reduces Q-factors [31] and the introduction of shapes onto the ground plane can improve the matching of antennas [32, 33].

The bottom layer of the antenna structure is shown in Figure 8. The initial size of the ground-plane, WGP, is $21 \times 22\,\text{mm}$, which covers the entire bottom layer of the antenna. Reducing the size of the

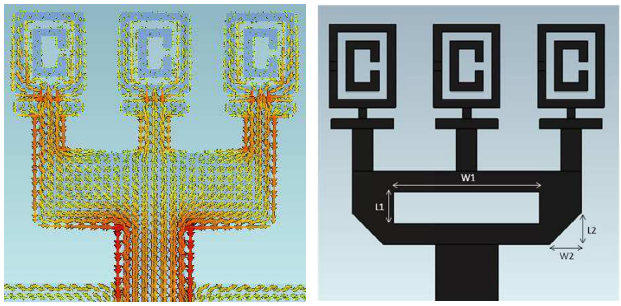

Figure 11. (a) The surface current distribution of the antenna, and (b) the etched-out area that corresponds to area of low surface current distribution.

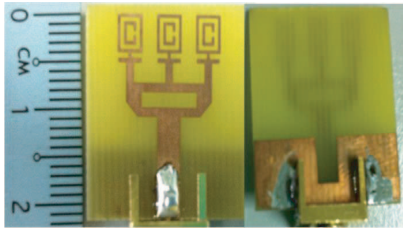

Figure 12. The fabricated antenna.

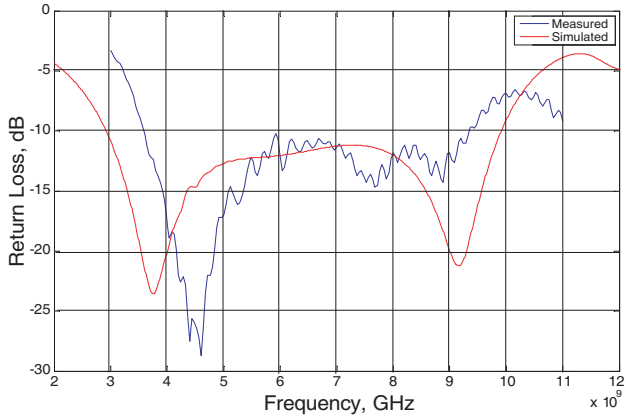

Figure 13. Comparisons between the measured and simulated return loss of the final (etched-out) antenna.

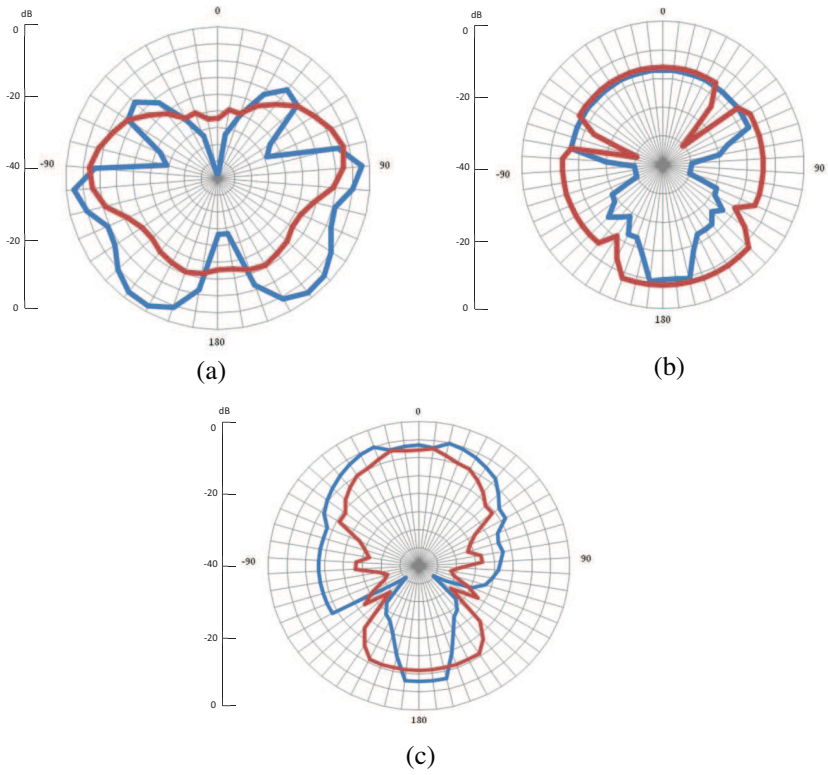

Figure 14. The measured radiation patterns in the xy-plane (blue line) and the yz-plane (red line), at (a) 3 GHz, (b) 6.5 GHz, and (c) 10 GHz.

ground plane in the positive x-direction, beginning from the radiating edge of the antenna, creates a partial ground plane. The result of a parametric study on the size of the partial ground plane is shown in Figure 9. A partial ground plane improves the matching of the LH modes $m = -1$ (at 7.82 GHz) and $m = -2$ (at 4.12 GHz). A partial ground plane with, $WGP = 7.5$ mm, matches the LH modes with losses below -10 dB each. The bandwidth at each resonating frequency increases, suggesting that a wide bandwidth can be achieved by proper matching throughout the band. A rectangular slot of length LS and width WS was therefore introduced to the center of the partial ground plane, as shown in Figure 8. Optimization of LS and WS yields wideband matching as shown in Figure 10(b). The bandwidth ratio (below -10 dB), taken at the lowest point of return loss (4.6 GHz,

−35 dB) is 133%.

To further reduce the stored energy, which contributes to the Q-factor, selected metallic areas were removed from the antenna. These removals reduce the surface area of the metallic plate, which in turn reduces the energy stored in the form of an electric field [34]. Metal removal was guided by an analysis of the surface current density on the antenna.

Areas with lower surface current density are etched out to reduce the total stored energy. The surface current distribution on the antenna is shown in Figure 11(a), where the color yellow indicates low magnitude surface current. The etched-out areas are the middle of the trident feed and its two corners, as shown in Figure 11(b). The relevant dimensions of the etched-out areas are as follows: $W_1 = 7$ mm, $L_1 = 1.5$ mm, $W_2 = 1.5$ mm and $L_2 = 1.5$ mm. The new, etched-out structure was analyzed, and the return loss is shown in Figure 10(c). The bandwidth ratio (below −10 dB), taken at the lowest point of return loss (3.7 GHz, −24 dB) is 189%. The −10 dB point of the antenna spans between 2.9–9.9 GHz, which makes it well suited to UWB applications.

To verify the wideband result, the antenna was fabricated and measured using the Agilent Technologies N5230A PNA-L Network Analyzer. The fabricated antenna is shown in Figure 12. Figure 13 shows a verification of the wideband result. The discrepancies between the measured and simulated antenna can be attributed to the fabrication and soldering accuracy. The measured radiation patterns of the antenna in the xy and yz-plane are shown in Figure 14 for three frequencies within the resonance range of the antenna. The gain of the antenna increases linearly between −1 dB to 5 dB throughout the frequency band, which can be attributed directly to the decreasing wavelength and the difference in field response on the aperture of the antenna throughout the band [35].

5. CONCLUSIONS

A compact MTM UWB antenna is proposed. The antenna exhibits a wide bandwidth of 189% at the resonance point of 3.7 GHz, spanning from 2.9–9.9 GHz (below −10 dB), making it suitable for use in the FUWB band defined by the Federal Communication Commission (FCC). The antenna consists of three LHM unit cells that combine a modified SRR structure with CLS. The left-handedness of the unit cells is demonstrated by the 1D and 2D dispersion diagrams. The eigencurrents corresponding to the resonating modes are excited using the proper matching techniques. More specifically, the RH and LH

resonant modes are properly matched by a trident feed and a slotted-partial ground plane, respectively. Parts of the structure are removed, guided by an analysis of the surface current distribution of the antenna in an effort to reduce the antenna's Q-factor. This modification leads to the wide bandwidth of the antenna.

REFERENCES

1. Xu, F., Z.-X. Wang, X. Chen, and X.-A. Wang, "Dual band-notched UWB antenna based on spiral electromagnetic-bandgap structure," *Progress In Electromagnetics Research B*, Vol. 39, 393–409, 2012.
2. Tilanthe, P., P. C. Sharma, and T. K. Bandopadhyay, "A compact UWB antenna with dual band rejection," *Progress In Electromagnetics Research B*, Vol. 35, 389–405, 2011.
3. Khaled, E. E. M., A. A. R. Saad, and D. A. Salem, "A proximity-FED annular slot antenna with different a band-notch manipulations for ultra-wide band applications," *Progress In Electromagnetics Research B*, Vol. 37, 289–306, 2012.
4. Chen, H., Y. Ding, and D. S. Cai, "A CPW-fed UWB antenna with WiMAX/WLAN band-notched characteristics," *Progress In Electromagnetics Research*, Vol. 25, 163–173, 2011.
5. Lin, S., R.-N. Cai, G.-L. Huang, and J.-X. Wang, "A miniature UWB semi-circle monopole printed antenna," *Progress In Electromagnetics Research Letters*, Vol. 23, 157–163, 2011.
6. Islam, M. T., R. Azim, and A. T. Mobashsher, "Triple band-notched planar UWB antenna using parasitic strips," *Progress In Electromagnetics Research*, Vol. 129, 161–179, 2012.
7. Yazdi, M. and N. Komjani, "A compact band-notched UWB planar monopole antenna with parasitic elements," *Progress In Electromagnetics Research*, Vol. 24, 129–138, 2011.
8. Osman, M. A. R., M. K. A. Rahim, M. Azfar, N. A. Samsuri, F. Zubir, and K. Kamardin, "Design, implementation and performance of ultra-wideband textile antenna," *Progress In Electromagnetics Research B*, Vol. 27, 307–325, 2011.
9. Zhou, D., S.-C. S. Gao, F. Zhu, R. A. Abd-Alhameed, and J.-D. Xu, "A simple and compact planar ultra wideband antenna with single or dual band-notched characteristics," *Progress In Electromagnetics Research*, Vol. 123, 47–65, 2012.
10. Malik, J. and M. V. Kartikeyan, "Metamaterial inspired patch antenna with L-shape slot loaded ground plane for dual band

(WiMAX/WLAN) applications," *Progress In Electromagnetics Research Letters*, Vol. 31, 35–43, 2012.

11. Mahdy, M. R. C., M. R. A. Zuboraj, A. A. N. Ovi, and M. A. Matin, "Novel design of triple band rectangular patch antenna loaded with metamaterial," *Progress In Electromagnetics Research Letters*, Vol. 21, 99–107, 2011.
12. Jing, N., H. Zhao, and L. Huang, "A novel design of planar spiral antenna with metamaterial," *PIERS Proceedings*, 725–728, Xi'an, China, Mar. 22–26, 2010.
13. Mahdy, M. R. C., M. R. A. Zuboraj, A. A. N. Ovi, and M. A. Matin, "Novel concept of ENG metamaterial in rectangular microstrip patch antenna (partially loaded case) for dual band application," *PIERS Proceedings*, 920–923, Marrakesh, Morocco, Mar. 20–23, 2011.
14. Du, G.-H., X. Tang, and F. Xiao, "Tri-band metamaterial-inspired monopole antenna with modified S-shaped resonator," *Progress In Electromagnetics Research Letters*, Vol. 23, 39–48, 2011.
15. Lee, H.-M. and H. Lee, "A dual-band metamaterial absorber based with resonant-magnetic structures," *Progress In Electromagnetics Research Letters*, Vol. 33, 1–12, 2012.
16. Danaeifar, M., M. Kamyab, A. Jafargholi, and M. Veysi, "Bandwidth enhancement of a class of cloaks incorporating metamaterials," *Progress In Electromagnetics Research Letters*, Vol. 28, 37–44, 2012.
17. Lee, C. J., K. M. K. H. Leong, and T. Itoh, "Composite right/left-handed transmission line based compact resonant antennas for RF module integration," *IEEE Trans. Antennas and Propag.*, Vol. 54, No. 8, 2283–2291, Aug. 2006.
18. Lee, C. J., K. M. K. H. Leong, and T. Itoh, "Design of resonant small antenna using composite right/left-handed transmission line," *Antennas Propagat. Soc. Int. Symp.*, Vol. 2B, 2005.
19. Caloz, C. and T. Itoh, *Electromagnetic Metamaterials: Transmission Line Theory and Microwave Applications — The Engineering Approach*, Wiley Interscience, 2006.
20. Shelby, R. A., D. R. Smith, and S. Schultz, "Experimental verification of a negative index of refraction," *Science*, Vol. 292, 77–79, Apr. 2001.
21. Lai, A., C. Caloz, and T. Itoh, "Composite right/left-handed transmission line metamaterials," *IEEE Microwave Magazine*, Vol. 5, No. 3, 34–50, Sep. 2004.
22. Pendry, J. B., A. J. Holden, D. J. Robbins, and W. J. Stewart,

"Magnetism from conductors and enhanced non-linear phenomena," *IEEE Trans. Microwave Theory Tech.*, Vol. 47, 2075–2084, Feb. 1999

23. Eleftheriades, G. V., "EM transmission-line metamaterials," *Materials Today*, Vol. 12, No. 3, 30–41, Mar. 2009
24. Majid, H. A., M. K. A Rahim, and T. Masri, "Microstrip antenna's gain enhancement using left-handed metamaterial structure," *Progress In Electromagnetic Research M*, Vol. 8, 235–247, 2009.
25. Tang, W. X., Q. Cheng, and T. J. Cui, "Electric and magnetic responses from metamaterial unit cells at Terahertz," *Terahertz Science and Technology*, Vol. 2, No. 1, Mar. 2009
26. Li, L., H. Yao, Q. Wu, and Z. Chen, "Broad-bandwidth and low-loss metamaterials: Theory, design and realization," *J. Zhejiang Univ. Science A*, Vol. 7, No. 1, 5–23, Jan. 2006.
27. Palandoken, M., A. Grede, and H. Henke, "Broadband microstrip antenna with left-handed metamaterials," *IEEE Trans. Antennas Propagat.*, Vol. 57, No. 2, 331–338, Feb. 2009.
28. Liu, J., K. P. Esselle, and S. Zhong, "An extremely wideband rectangular monopole antenna with a modified microstrip feed," *Proc. Antennas and Propagation, (EuCAP)*, 1–5, Apr. 2010
29. Yaghjian, A. D. and S. R. Best, "Impedance, bandwidth, and Q of antennas," *IEEE Trans. Antennas Propagat.*, Vol. 53, No. 4, 1298–1324, 2005.
30. Gustafsson, M. and S. Nordebo, "Bandwidth, Q factor, and resonance models of antennas," *Progress In Electromagnetic Research*, Vol. 62, 1–20, 2006.
31. Yang, H. Y. D. and Y. Y. Zhang, "A wideband miniaturized dipole antenna on a printed circuit board," *Progress In Electromagnetic Research C*, Vol. 10, 175–185, 2009.
32. Chen, Z. N., T. S. P. See, and X. Qing, "Small printed ultrawideband antennas with reduced ground plane effect," *IEEE Trans. Antennas Propagat.*, Vol. 55, No. 2, 383–388, 2007.
33. Sadat, S., M. Fardis, F. G. Kharakhili, and G. Dadashzadeh, "A compact microstrip square-ring slot antenna for UWB applications," *Progress In Electromagnetic Research*, Vol. 67, 173–179, 2007.
34. Hayt, Jr., W. H. and J. A. Buck, *Engineering Electromagnetics*, 6th edition, McGraw Hill, 2001.
35. Kraus, J. D. and R. J. Marhefka, *Antennas for All Applications*, 3rd edition, McGraw-Hill, 2003.